

Article

Transient Stability Analysis of Grid-Connected Converter Driven by Imbalance Power under Non-Severe Remote Voltage Sag

Xuli Quan , Xinchun Lin *, Yun Zheng and Yong Kang

State Key Laboratory of Advanced Electromagnetic Engineering and Technology (AEEET), School of Electrical and Electronic Engineering (SEEE), Huazhong University of Science and Technology (HUST), Wuhan 430074, China; quanxuli@hust.edu.cn (X.Q.); yunzheng@hust.edu.cn (Y.Z.); ykang@mail.hust.edu.cn (Y.K.)

* Correspondence: linxinchun@mail.hust.edu.cn

Abstract: In the transient process of the grid-connected converter (GCC), the existing research mainly focuses on the impact of the control loops. Little attention is paid to the transient stability issues driven by the imbalance between the input power and output power of GCC. This paper shows that the transient stability issues will still exist even if ignoring the dynamics of phase-locked loop (PLL) and current loop. In this paper, the models of the AC grid and the GCC are built under the assumption that the dynamics of the PLL and current loop are ignored. Then, by analyzing the transient process of GCC under non-severe remote voltage sag, the effects of the imbalance power on the transient stability of GCC are discussed. Moreover, for the GCC to operate stably after the transient process, there should be a maximum input power limit (MIPL) for GCC, and the imbalance power equation is applied in this paper to determine the transient stability of GCC. Furthermore, the effects of the current limitation on the transient stability of the GCC are also discussed. Finally, the theoretical analysis has been verified by means of simulations.

Keywords: grid-connected converter; imbalance power; non-severe remote voltage sag; maximum input power limit (MIPL); current limitation; imbalance power equation



Citation: Quan, X.; Lin, X.; Zheng, Y.; Kang, Y. Transient Stability Analysis of Grid-Connected Converter Driven by Imbalance Power under Non-Severe Remote Voltage Sag. *Energies* **2021**, *14*, 1737. <https://doi.org/10.3390/en14061737>

Academic Editor: Pedro Roncero-Sanchez

Received: 18 January 2021
Accepted: 12 March 2021
Published: 21 March 2021

Publisher's Note: MDPI stays neutral with regard to jurisdictional claims in published maps and institutional affiliations.



Copyright: © 2021 by the authors. Licensee MDPI, Basel, Switzerland. This article is an open access article distributed under the terms and conditions of the Creative Commons Attribution (CC BY) license (<https://creativecommons.org/licenses/by/4.0/>).

1. Introduction

With increasing environmental problems and a severe energy crisis, the proportion of renewable energy in the power system is increasing each year. Wind power and photovoltaic are the two main forms of renewable energy generation in the power system [1]. A large part of these two renewable energy sources are connected to the transmission grid by the grid-connected converters (GCCs) [2–4]. Thus, the stability of the power system is largely influenced by the GCC. In some places of the world, such as in China, these renewable energy resources are usually located in remote areas, which leads to GCCs connected to a weak AC grid. The weak grid condition makes the stability of GCC face a greater challenge [5–7].

In order to avoid the renewable energy generation disconnecting with the AC grid during the grid faults, the GCC must maintain transient stability. However, when the grid faults happen, even when it is a non-severe grid fault, the GCC may become unstable and the renewable energy generation will be cut off from the grid, which will lead to the loss of renewable energy. To avoid such a situation, the transient process of GCC under the grid faults requires deeper research.

Most of the previous studies pay attention to the influence of the control system during the transient process of GCC. Different control strategies and different control parameters will lead to the different performance of the control loops.

The influence of the parameters of the phase-locked loop (PLL) on the transient stability of the GCC is analyzed in References [8–10]. Based on the mathematical analysis

of the PLL, the transient responses of the GCC with different PLL parameters are analyzed in Reference [8]. In Reference [9], by comparing with the rotor motion model of the synchronous generator, a nonlinear model of the PLL is developed and the equal-area criterion is carried out to analyze the transient stability of GCC. In Reference [10], by analyzing the behavior of the PLL under different grid impedance, a general quasi-static model of PLL is built and the influence factors on the stability of GCC are presented.

In References [11,12], the impact of the parameters of the inner current loop is analyzed. Reference [11] investigates the mechanism of the electrical oscillations in the GCC connected with weak grid system by analyzing the damping characteristics of the current controller and PLL, while Reference [12] holds the view that the current loop does not have a significant impact on the transient stability of the power system since it is much faster than other control loops. The current limitation, which is being introduced in GCC to protect the switching devices from being damaged by the overcurrent, also have effects on the transient stability of GCC [13–15].

These previous studies above mainly focus on the influence of the PLL and the current loop [16,17]. However, the influence of the PLL and the current loop is not the only influence factor on the transient stability of the GCC. Actually, even if the dynamics of the PLL and the current loop are ignored, the system stability issues will still exist because of the imbalance power caused by the grid faults. As for the influence of the current limitation on the transient stability of GCC, the main reason why current limitation has an impact on the transient stability of GCC is that current limitation will affect the imbalance power, while the imbalance power will affect the transient stability of GCC. Therefore, none of these previous studies shows the impact of the imbalance power, although the imbalance power is a vital influence factor on the transient stability of GCC. Moreover, since the main function of the GCC is to perform power conversion, the most basic characteristics of the GCC are mainly reflected in its capability of power conversion. Thus, when the GCC becomes unstable during the transient process, perhaps it is because of the imbalance power, but not the parameters of the control loops.

Except for the PLL and the current loop, References [18–20] analyze the transient stability of GCC, including the outer voltage loop by using the nonlinear analysis method. The nonlinear analysis method is a kind of commonly used mathematical method in transient stability problems and this kind of method can get an accurate result [21]. However, the full-order models of the GCC applied in these papers are complex. When these kinds of models are applied to analyze the transient stability of GCC, the analysis process becomes very complicated and it is not easy to figure out the key influence factors on these transient stability issues. The impact of the imbalance power during the transient process of GCC cannot be intuitively reflected in these models.

It can be seen that the previous studies either only consider PLL and current loop, or establish overly complex full-order models. However, how to analyze the transient stability of GCC and its key influence factors when the dynamics of the PLL and the current loop are ignored is still a big issue. Therefore, a simple and clear mathematical model of GCC that can show the key influence factors of the transient stability of GCC is needed, which is a big challenge. This paper is going to discuss these issues from the perspective of imbalance power, which is rarely done according to these previous studies.

When analyzing the transient process of GCC, it can be compared with the synchronous generators (SG). The conventional SGs transfer the mechanical power into electromagnetic power through the rotation of the rotor [22,23], while the GCC keeps power balancing through its DC capacitor. Although the energy transmission media of the SG and GCC are different, the effects of the imbalance power may be similar [24–26]. Thus, the rotor motion equation of SG can still be referred when building the mathematical model of GCC [27]. Actually, in the later part of this paper, it can be seen that the form of the mathematical model of GCC is similar with the rotor motion equation of SG.

In this paper, a mathematical model of GCC is developed, and the effects of the imbalance power are presented. A greater imbalance power will have a greater impact

on the transient stability of GCC. Therefore, to keep the GCC maintain transient stability under the grid faults, the input power should be limited. Meanwhile, the current limitation will also have some influence on the transient stability of GCC since the current limiter will have some effects on the imbalance power. It is also discussed in this paper. Moreover, the imbalance power equation is proposed in this paper to determine the transient stability of GCC.

The rest part of this paper is organized as follows. In Section 2, based on the analysis of the equivalent AC circuit of the power system with GCC and the output power characteristics, the modeling of the AC grid and the mathematical model of GCC are discussed. In Section 3, the details about the transient process of GCC with non-severe grid faults are analyzed. The imbalance power equation of GCC is carried out in Section 4. The simulations and experimental verifications in Section 5 prove the correctness of the theoretical analysis. Finally, the conclusions are drawn in Section 6.

2. Modeling of the AC Grid and the Grid-Connected Converter

The power system with a single GCC can be separated into two parts, one is the AC grid, and another is the GCC. Thus, in this part, the modeling of the AC grid and the mathematical model of GCC will be discussed. Since the characteristics of the output power are essential for analyzing the impact of the imbalance power, the following section will focus on them.

A typical control diagram of GCC connected to the AC grid is shown in Figure 1. The control strategy of GCC consists of the inner current loop, outer DC voltage loop, and the PLL. The active power flow of GCC is controlled by the DC voltage loop and active current loop. The reactive current loop aims at tracking reactive current commands, for the sake of simplicity, ignoring the outer AC-voltage loop or reactive power loop. PLL is used to synchronize GCC with the AC grid. The d-axis of the synchronous reference frame is oriented on the point of common coupling (PCC) voltage vector U_t by PLL. It has to be mentioned that the AC grid here refers to the transmission grid. Distribution network is not considered. Therefore, only inductive grids are considered in this paper.

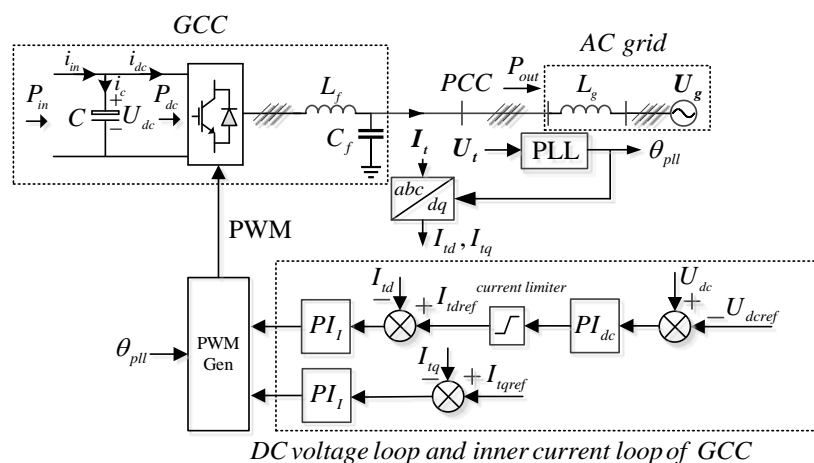


Figure 1. The typical control diagram of grid-connected converter (GCC) connected to the AC grid.

2.1. Modeling of the AC Grid

By ignoring the dynamics of the AC grid, the fundamental frequency equivalent AC circuit of GCC connected to the AC grid can be obtained from the control diagram. Considering that the d -axis and q -axis components of AC current, I_{td} and I_{tq} , are fully controllable by the current control loop, the GCC can be equivalent to a current source. Figure 2 shows the equivalent circuit.

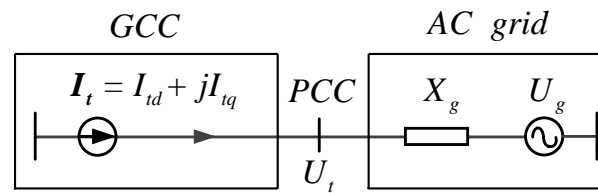


Figure 2. Equivalent AC circuit of GCC connected to the AC grid.

According to the equivalent AC circuit of GCC connected to the AC grid, the relationship of different vectors is shown in Figure 3. Grid voltage U_g falls behind the PCC voltage U_t by an angle of δ_t . Taking the phase of U_t as a reference, and U_t can be expressed as $U_t \angle 0$, while U_g can be expressed as $U_g \angle -\delta_t$.

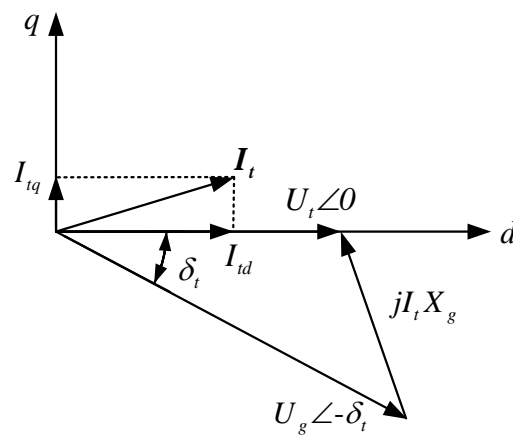


Figure 3. The relationship of various vectors under the phase-locked loop (PLL) synchronous reference frame.

According to Figure 3, the mathematical relationship between the amplitude of the PCC voltage and the grid voltage can be expressed as Equation (1), and the expression of output power can be expressed as Equation (2).

$$U_t = \sqrt{U_g^2 - I_{td}^2 X_g^2} - I_{tq} X_g \quad (1)$$

$$P_{out} = \frac{3}{2} (U_{td} I_{td} + U_{tq} I_{tq}) \quad (2)$$

In Equation (2), the U_{td} and U_{tq} are the d -axis and q -axis components of PCC voltage, respectively. As mentioned before, the d -axis is oriented on the PCC voltage by PLL. Thus, if ignoring PLL dynamics, the q -axis component of PCC voltage U_{tq} should be equal to zero. That means when substituting Equation (1) into Equation (2), the expression of output power can be derived as Equation (3).

$$P_{out} = \frac{3}{2} \left(\sqrt{U_g^2 - I_{td}^2 X_g^2} - I_{tq} X_g \right) I_{td} \quad (3)$$

From Equation (3), it can be known that the output power is determined by the grid voltage, grid-side equivalent impedance, and d -axis and q -axis components of the AC current. Since the fluctuations of the grid voltage and grid-side equivalent impedance cannot be large during the transient process, the grid voltage and the grid-side equivalent impedance are considered constant in the power system. Therefore, the relationship between the output power and the AC current can be defined as the output power characteristics. Figure 4 shows the output power characteristic curve under the condition that $I_{tq} = 0$, so the output power characteristic curve can also be called the P_{out} - I_{td} curve.

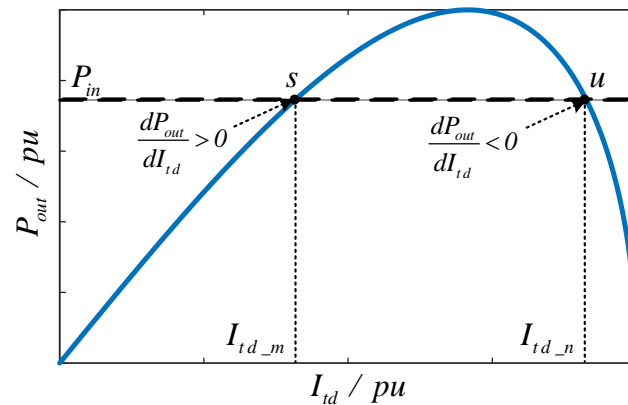


Figure 4. Output power characteristic curve ($I_{tq} = 0$).

2.2. Mathematical Model of GCC

Ignoring the power loss of GCC, then $P_{dc} = P_{out}$, and Equation (4) can be derived from the DC side of GCC according to Figure 1.

$$C \frac{dU_{dc}}{dt} = i_{in} - i_{dc} = \frac{P_{in} - P_{dc}}{U_{dc}} = \frac{P_{in} - P_{out}}{U_{dc}} \quad (4)$$

According to the DC voltage loop shown in Figure 1, Equation (5) can be derived based on the assumption that ignoring the dynamics of the current loop. The k_{vp} and k_{vi} are the proportion and integration parameters of the DC voltage loop PI controller.

$$I_{td} = (U_{dc} - U_{dcref}) \left(k_{vp} + \frac{k_{vi}}{s} \right) \quad (5)$$

Converting Equation (5) into the time-domain expression, Equation (6) can be obtained.

$$\frac{dI_{td}}{dt} = k_{vi} (U_{dc} - U_{dcref}) + k_{vp} \frac{d(U_{dc} - U_{dcref})}{dt} \quad (6)$$

Combining Equations (4) and (6), the mathematical model of GCC can be obtained and it is shown as Equation (7).

$$\begin{cases} \frac{dI_{td}}{dt} = k_{vi} (U_{dc} - U_{dcref}) + k_{vp} \frac{d(U_{dc} - U_{dcref})}{dt} \\ C \cdot U_{dc} \frac{dU_{dc}}{dt} = P_{in} - P_{out} \end{cases} \quad (7)$$

The active power control is considered in Equation (7). If the reactive power is considered, the order of the mathematical model of GCC will be higher, which will make the analysis become more complex. In order to simplify the analysis, the reactive current I_{tq} is not taken into consideration.

According to the mathematical model of the GCC and the modeling of the AC grid, the stable operating point of GCC can be analyzed. As shown in Figure 4, two intersections of input power P_{in} and the output power characteristic curve are the possible operating points. At point s , when a small disturbance occurs, the output power P_{out} will be influenced and it will have a slight change. If P_{out} increases, both the DC voltage U_{dc} and the active current I_{td} will begin to decrease according to Equation (7). Later, since $dP_{out}/dI_{td} > 0$ at point s , P_{out} will decrease with the decrease of I_{td} . As a result, the operating point will return back to the point s , which means the point s is a stable operating point. However, since $dP_{out}/dI_{td} < 0$ at point u , the DC voltage loop will become a positive feedback loop when a small disturbance occurs, which means that point u is an unstable operating point. Therefore, if the system operates stably, the operating point must satisfy the condition that $dP_{out}/dI_{td} > 0$.

3. Analysis of the Transient Process of Grid-Connected Converter Driven by the Imbalance Power

When the remote voltage sag happens, there will be a sudden voltage drop of the AC grid as shown in Figure 5, which will lead to a sudden change of the output power while the output current keeps unchanged. From Figure 6, it can be known that under a severe voltage sag fault, there will be no intersections between the input power P_{in} and the $P_{out}-I_{td}$ curve. In such a case, there is no chance for GCC to operate stably, because there is no operating point for GCC after the fault. Only when the grid fault is not very severe, the input power and the output power characteristic curve will have intersections. Furthermore, since the non-severe voltage sag will not make the PCC voltage have too much change, the control strategy of GCC will not switch to the LVRT control strategy and it will maintain the typical control strategy as shown in Figure 1. Only under such a condition, there is the possibility for GCC to operate stably. Thus, only non-severe grid faults are discussed here.

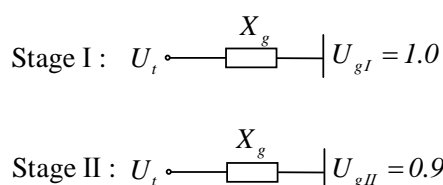


Figure 5. Equivalent AC circuits of GCC connected to the AC grid under different operating stages.

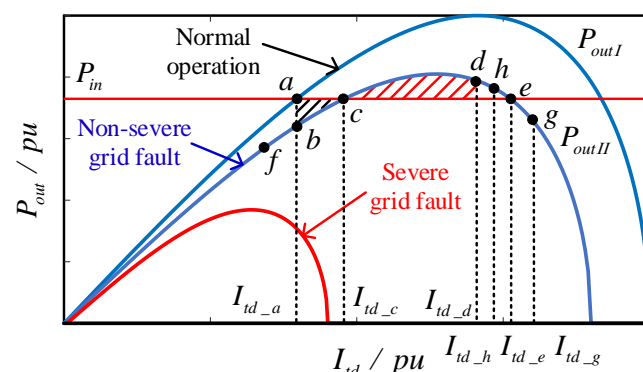


Figure 6. Different output power characteristic curves under severe and non-severe remote voltage sag.

As shown in Figure 5, before the remote voltage sag occurs (defined as stage I), the system operates normally, and the corresponding output power characteristic curve is P_{outI} as shown in Figure 6. After the remote voltage sag occurs (defined as stage II), the corresponding output power characteristic curve changes into P_{outII} . The imbalance power caused by the fault will lead to an oscillation of the active current I_{td} and DC voltage U_{dc} , which may make the power system become unstable. The details about the transient process are explored in the following parts.

3.1. Analysis of the Stable Transient Process

As mentioned before, when the system operates stably, the operating point must meet the condition that $dP_{out}/dI_{td} > 0$. Thus, in stage I, the operating point should be the point a as shown in Figure 6. When the remote voltage sag occurs, considering that I_{td} is the AC current flowing through the grid-side equivalent inductor so I_{td} cannot change instantly after the fault occurs. Thus, the operating point will suddenly change from a to b . Since the input power P_{in} is now larger than the output power P_{out} , the DC side capacitor C begins to charge and store energy and DC voltage U_{dc} will increase.

Then, the active current will increase under the action of the DC voltage loop. When the active current reaches I_{td_c} , P_{in} is equal to P_{out} but U_{dc} is still larger than its reference

value $U_{dc_{ref}}$. Hence, with the control of the DC voltage loop, the active current will keep increasing, and P_{out} begins to be larger than P_{in} . As P_{out} begins to be larger than P_{in} , the DC side capacitor starts to release energy and U_{dc} begins to decrease. When U_{dc} decreases to $U_{dc_{ref}}$, the active current reaches its peak value I_{td_d} and the operating point runs to the point d .

Since P_{out} is still larger than P_{in} at point d , the DC side capacitor continues to release energy and U_{dc} will keep decreasing. As U_{dc} continues to decrease, U_{dc} begins to be smaller than $U_{dc_{ref}}$ and the active current begins to decrease. When the active current decreases to I_{td_c} , P_{in} begins to be larger than P_{out} , and U_{dc} starts to rise. When U_{dc} increases to $U_{dc_{ref}}$, the operating point runs to the point f and the system starts the second oscillation process.

If there is no energy loss during the oscillation, the operating point will keep running indefinitely between the point f and the point d on the output power characteristic curve P_{outII} . Considering the existence of various damping effects in this transient process, the oscillation amplitude will gradually decay, and the GCC will finally operate at a stable operating point c .

3.2. Analysis of the Unstable Transient Process

It can be seen from Figure 6 that the point e is another intersection of P_{in} and $P_{out II}$. The analysis above is based on the condition that the active current cannot reach I_{td_e} in the first oscillation process. However, if the active current increases beyond I_{td_e} in the first oscillation process, U_{dc} will continue to increase and will never return back to its reference value since P_{in} is larger than P_{out} after point e . This can also be explained from a more intuitive perspective: the energy gained by the DC capacitor has not yet been completely released when the operating point reaches point e . Consequently, U_{dc} is still larger than its reference value $U_{dc_{ref}}$ and it continues to increase. Then, U_{dc} will rise fast under the imbalance power and it can never return back to its reference value $U_{dc_{ref}}$. Finally, the system becomes unstable.

To maintain stable operation during the transient process, the operating point of GCC cannot run over the point e in the first oscillation process. The larger the input power, the easier it is for the operating point to run across the point e . Therefore, there should be a maximum input power limit (MIPL) for the GCC to keep stable after the transient process. If the input power is larger than the MIPL, the GCC cannot maintain stable operation after the grid fault.

Defining the imbalance power $\Delta P = P_{out} - P_{in}$. Although the waveforms of ΔP , U_{dc} , and I_{td} cannot be computed, their changing tendencies can be obtained through the analysis above. Then, their theoretical waveforms can be drawn qualitatively. By drawing these theoretical time-domain waveforms, the transient process will be much more intuitive. Based on the analysis above, the theoretical oscillation waveforms of ΔP , U_{dc} , and I_{td} during the transient process are shown in Figure 7.

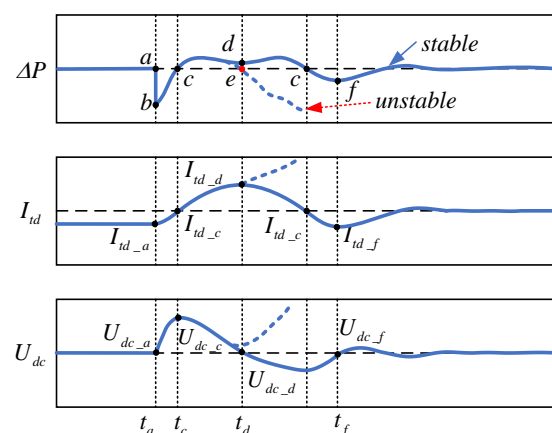


Figure 7. The theoretical oscillation waveforms of ΔP , U_{dc} , and I_{td} during the transient process.

3.3. Analysis of the Transient Process with the Current Limiter

In the situation of real application, the current references limiter is always adopted to avoid the overcurrent of the converter. Since the value of the current limitation usually depends on the ability of the GCC to withstand overcurrent, the effects of the current limitation on the imbalance power need to be discussed. The analysis of the transient process in the above two parts is based on the situation that the current does not reach the limit value. When the current reaches the current limitation, the influence of the current limiter during the transient process is analyzed as follows.

As shown in Figure 6, if the value of the current limitation is larger than I_{td_e} , such as I_{td_g} . When the current reaches the current limitation, P_{in} is larger than P_{out} . Since the current is limited to a constant, P_{out} also becomes a constant and the imbalance power ΔP becomes a constant. Thus, DC side capacitor will continue to be charged. The U_{dc} will continue to increase and never return back to its reference value. Finally, the converter will definitely become unstable. In this condition, the only way to keep GCC operating stably is to let the input power be smaller than the MIPL.

Nevertheless, if the current limitation is smaller than I_{td_e} , such as I_{td_h} . When the current reaches the limitation, the current will be limited and become a constant. According to Equation (3), the output power will also become a constant and the operating point will stay on point h as shown in Figure 6. Since the output power is always larger than the input power, the DC side capacitor will continue to release energy and U_{dc} will keep decreasing. When the output of the DC voltage loop is smaller than the current limitation, the current limiter will stop working and the current will decrease. Then, the operating point will oscillate between point f and point h . Finally, the converter will operate stably at point c .

It can be seen that the influence of the current limitation on the transient stability of GCC is reflected on its limitation of the imbalance power. Therefore, based on the analysis of how the imbalance power will influence the transient stability of the GCC, the influence of the current limitation on the transient stability of GCC can be obtained easily. If the current limiter limits the imbalance power to a constant before P_{in} is larger than P_{out} , the GCC can maintain stable operation. Otherwise, the GCC will become unstable. Based on the analysis above, the theoretical oscillation waveforms of ΔP , U_{dc} , and I_{td} during the transient process are shown in Figure 8.

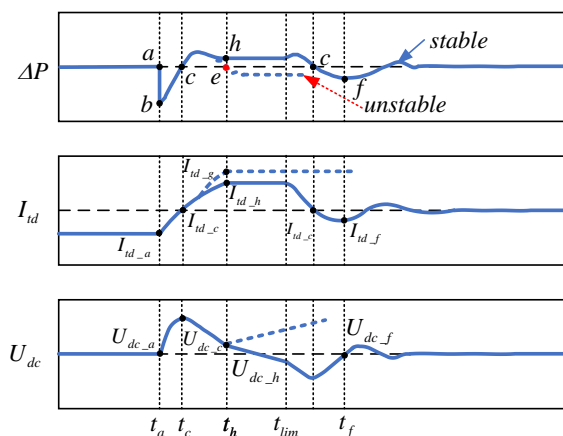


Figure 8. The theoretical oscillation waveforms of ΔP , U_{dc} , and I_{td} during the transient process with the current limiter.

4. Imbalance Power Equation

In order to determine whether the GCC will eventually become unstable or finally operate in a new stable operating point after the remote voltage sag, the imbalance power equation is proposed in this paper. On the basis of the mathematical model of the GCC, the

imbalance power equation can be derived and it can be used to determine the transient stability of GCC when a non-severe grid fault occurs.

$$C \cdot U_{dc} \frac{dU_{dc}}{dt} = P_{in} - P_{out} \quad (8)$$

$$\frac{dI_{td}}{dt} = k_{vi}(U_{dc} - U_{dcref}) + k_{vp} \frac{d(U_{dc} - U_{dcref})}{dt} \quad (9)$$

The first oscillation process lasts from t_a to t_d as shown in Figure 7. First, analyzing the transient process from t_a to t_c . Rewriting the mathematical model of GCC as Equations (8) and (9). For Equation (8), by integrating I_{td} on both sides, Equation (10) can be derived.

$$\int_{I_{td_a}}^{I_{td_c}} (P_{in} - P_{outII}) dI_{td} = C \cdot \int_{I_{td_a}}^{I_{td_c}} U_{dc} \frac{dU_{dc}}{dt} dI_{td} \quad (10)$$

From Equation (9), Equation (11) can be derived.

$$dI_{td} = k_{vi}(U_{dc} - U_{dcref}) dt + k_{vp} dU_{dc} \quad (11)$$

Substituting Equation (11) into Equation (10) and simplifying the equation, Equation (12) can be obtained. Here, the i_c is the DC capacitor current as shown in Figure 1.

$$\int_{I_{td_a}}^{I_{td_c}} (P_{in} - P_{outII}) dI_{td} - \frac{k_{vp}}{C} \int_{t_a}^{t_c} U_{dc} i_c^2 dt = k_{vi} C \cdot \int_{U_{dc_a}}^{U_{dc_c}} U_{dc} (U_{dc} - U_{dcref}) dU_{dc} \quad (12)$$

The item with k_{vp} in Equation (12) is always positive, and it can be regarded as the damping term. The right side of Equation (12) can be furtherly written as Equation (13).

$$\begin{aligned} & k_{vi} C \int_{U_{dc_a}}^{U_{dc_c}} U_{dc} (U_{dc} - U_{dcref}) dU_{dc} \\ & = k_{vi} C \left[\frac{(U_{dc_c} - U_{dcref})^3}{3} + \frac{U_{dcref} (U_{dc_c} - U_{dcref})^2}{2} \right] \end{aligned} \quad (13)$$

The physical meaning of the item $U_{dc} - U_{dcref}$ in Equation (13) is the change of DC voltage with respect to its reference value. Thus, the left part of Equation (13) indicates the energy change of the DC-side capacitor during the transient process.

As for the transient process from t_c to t_d , using the same analysis method and Equation (14) can be derived.

$$\begin{aligned} & \int_{I_{td_c}}^{I_{td_d}} (P_{in} - P_{outII}) dI_{td} - \frac{k_{vp}}{C} \int_{t_c}^{t_d} U_{dc} i_c^2 dt \\ & = -k_{vi} C \left[\frac{(U_{dc_c} - U_{dcref})^3}{3} + \frac{U_{dcref} (U_{dc_c} - U_{dcref})^2}{2} \right] \end{aligned} \quad (14)$$

Combining Equations (12) and (14), Equation (15) can be derived.

$$\int_{I_{td_a}}^{I_{td_c}} (P_{in} - P_{outII}) dI_{td} - \frac{k_{vp}}{C} \int_{t_a}^{t_d} U_{dc} i_c^2 dt = \int_{I_{td_c}}^{I_{td_d}} (P_{outII} - P_{in}) dI_{td} \quad (15)$$

Equation (15) can also be written in the form of imbalance power $\Delta P = P_{outII} - P_{in}$, as shown in Equation (16).

$$\int_{I_{td_c}}^{I_{td_a}} (\Delta P) dI_{td} - \frac{k_{vp}}{C} \int_{t_a}^{t_d} U_{dc} i_c^2 dt = \int_{I_{td_c}}^{I_{td_d}} (\Delta P) dI_{td} \quad (16)$$

According to Equation (16), the integration of the imbalance power in the left part is the area of the black shaded region abc as shown in Figure 6, which represents the energy-storage area of the DC side capacitor. The integration of the imbalance power in the right part of Equation (16) is the area of the red shaded region cdg as shown in Figure 6,

which represents the energy-releasing area of the DC side capacitor. The term related to k_{vp} in Equation (16) is the damping term of the system, and its effect on the GCC is similar to the positive damping sources' effect on the synchronous generators. The calculation of the damping term is complicated. In order to simplify the calculation, ignoring the damping term, then Equation (16) can be simplified to Equation (17).

$$\int_{I_{td_c}}^{I_{td_a}} (\Delta P) dI_{td} = \int_{I_{td_c}}^{I_{td_d}} (\Delta P) dI_{td} \quad (17)$$

Equation (17) is the practical form of the imbalance power equation. It can be used to determine the transient stability of the GCC when the remote voltage sag occurs. If the operating point runs to point e as shown in Figure 6, the system will be critically stable. The input power calculated by Equation (17) will be the MIPL of the GCC under such a condition. If the actual input power of the GCC is less than the MIPL, the system will be able to keep operating stably after the transient process. If the actual input power is larger than the MIPL, the system will be unstable when the fault occurs. As for the current limitation, it can be known that the I_{td_e} is the critical current limitation according to the analysis in the previous part. Since P_{in} is equal to P_{out} at point e , the critical current limitation I_{td_e} can be calculated by equation $\Delta P = 0$. Only when the current limitation is smaller than I_{td_e} , there is the possibility for the GCC to maintain transient stability.

Although the imbalance power equation can be used to determine the transient stability of GCC under the non-severe grid fault, the ignoring of the damping term will bring some errors. If $k_{vp} \neq 0$, the damping term in Equation (16) will always be positive. Therefore, the effect of the damping term will make the actual MIPL of the system become larger than the MIPL calculated by Equation (17), which means the results calculated by Equation (17) is conservative. Furthermore, a larger k_{vp} will make the damping term become larger. Meanwhile, the errors will also become larger.

5. Simulation and Experimental Results

To verify the theoretical analysis, a detailed simulation model of 2 MW GCC connected to the AC grid is built in MATLAB/Simulink. The simulation parameters are shown in Table 1. The imbalance power equation and the effects of the current limitation are verified in this simulation. Moreover, hardware-in-the-loop (HIL) experiments based on the SpaceR are carried out. The system parameters used in the experiments are the same with the simulation.

Table 1. Simulation and Experimental Parameters.

Symbol	QUANTITY	Value of the Quantity
P_{base}	Power base	2 MW
V_{base}	RMS line voltage base	690 V
f_{base}	Fundamental frequency	50 Hz
U_{dc}	DC voltage	1300 V
C	DC side capacitance	0.06 F
L_f, C_f	LC filter inductance and filter capacitance	0.075 mH, 960 μ F
k_{vp}, k_{vi}	DC voltage loop PI parameters	6/7, 170
k_{ip}, k_{ii}	Current loop PI parameters	0.2, 355
k_{pll}, k_{plli}	PLL PI parameters	0.15, 25
U_{gI}	Grid voltage in stage I (pu)	1.0
U_{gII}	Grid voltage in stage II (pu)	0.9

5.1. The Verification of the Imbalance Power Equation

If the overcurrent does not reach the current limitation and the current limiter does not work, there should be a MIPL for the GCC to operate stably. In this simulation, the grid voltage drops from 1.0 pu to 0.9 pu when the remote voltage sag happens at $t = 0.5$ s. Four cases are given in this simulation. In the first case, the short circuit ratio (SCR) of the system

is 1.9 and k_{vp} is 6. When the input power is 0.754 pu, the system is critically stable and Figure 9a shows the simulation waveforms of ΔP , I_{td} , and U_{dc} . If the input power is slightly larger, such as when the input power is 0.755 pu, the system becomes unstable as shown in Figure 9b. Thus, the MIPL obtained by the simulation is 0.754 pu when SCR = 1.9. In the second case, the SCR and k_{vp} of this system are 2.0 and 6, respectively. The simulation process is similar to the first case. From Figure 9c,d, it can be known from the simulation that the MIPL of the system is 0.794 pu. The SCR and k_{vp} in the third case are 2.0 and 7, respectively. From Figure 9e,f, it can be known the MIPL is 0.795 pu in this case. In the last case, the SCR and k_{vp} are 2.0 and 9, respectively. From Figure 9g,h, it can be known the MIPL is 0.796 pu in this case. Furthermore, when k_{vp} is 6, the approximate relationship between the MIPL and the SCR is sketched by drawing points as shown in Figure 9i. It can be seen that as SCR becomes larger, the MIPL becomes larger, which means a stronger grid will have a stronger anti-interference ability. It can also be seen that the MIPLs calculated by the imbalance power equation are always smaller than the simulation results, which is consistent with the analysis of the effects of damping term.

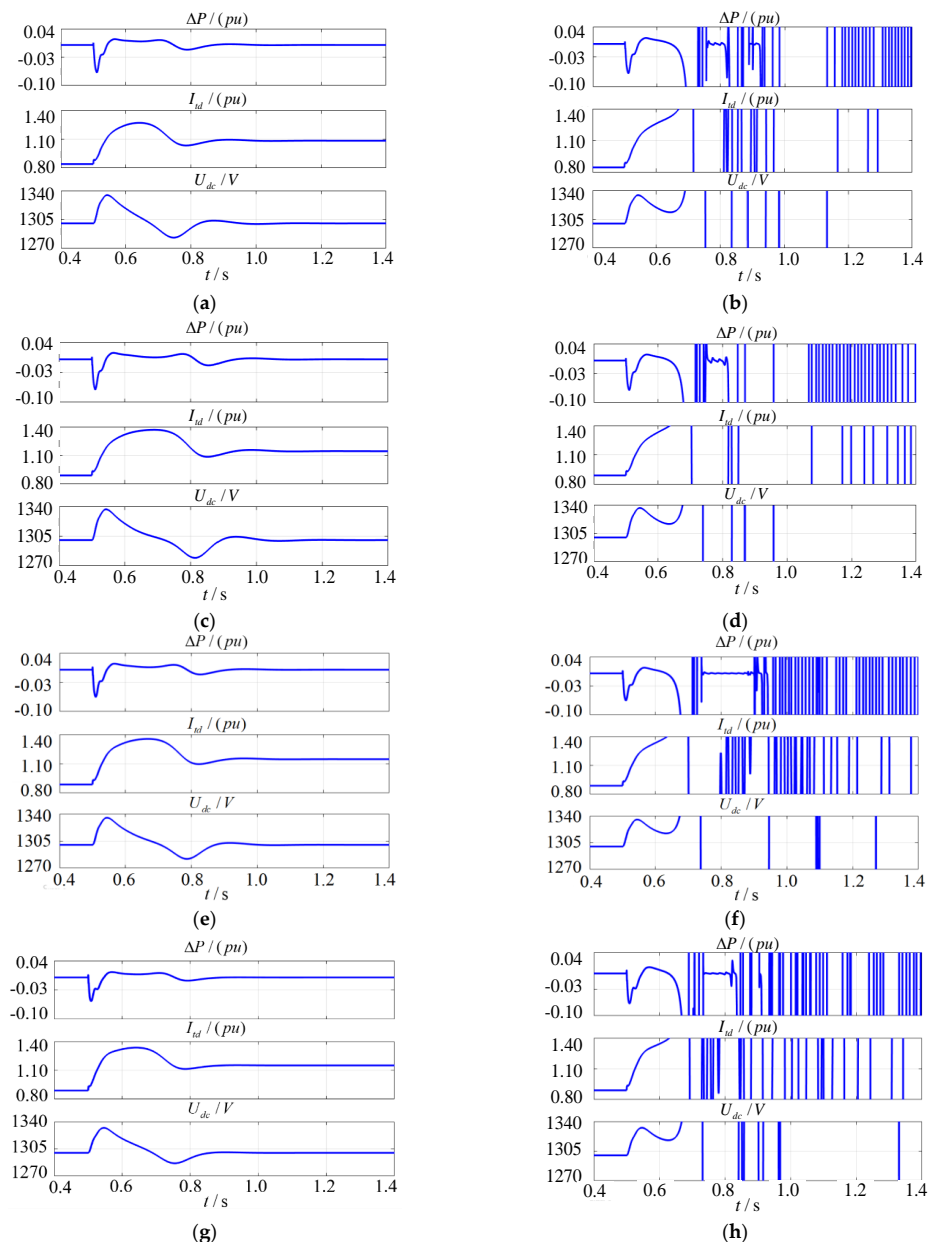


Figure 9. Cont.

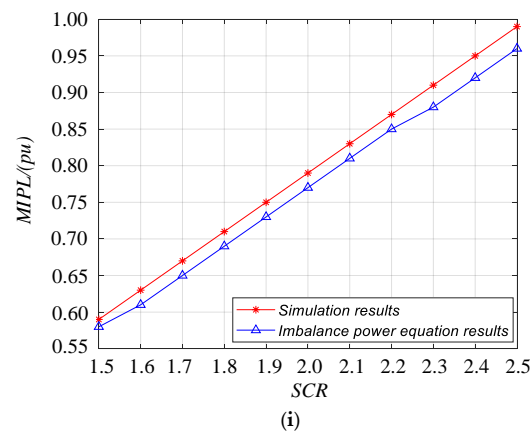


Figure 9. The simulation results when the remote voltage sag occurs: **(a)** The system is critically stable ($P_{in} = 0.754$ pu, SCR = 1.9, $k_{vp} = 6$); **(b)** The system is unstable ($P_{in} = 0.755$ pu, SCR = 1.9, $k_{vp} = 6$); **(c)** The system is critically stable ($P_{in} = 0.794$ pu, SCR = 2.0, $k_{vp} = 6$); **(d)** The system is unstable ($P_{in} = 0.795$ pu, SCR = 2.0, $k_{vp} = 6$); **(e)** The system is critically stable ($P_{in} = 0.795$ pu, SCR = 2.0, $k_{vp} = 7$); **(f)** The system is unstable ($P_{in} = 0.796$ pu, SCR = 2.0, $k_{vp} = 7$); **(g)** The system is critically stable ($P_{in} = 0.796$ pu, SCR = 2.0, $k_{vp} = 9$); **(h)** The system is unstable ($P_{in} = 0.797$ pu, SCR = 2.0, $k_{vp} = 9$); **(i)** Relationship between short circuit ratio (SCR) and maximum input power limit (MIPL) when $k_{vp} = 6$.

Comparing with the theoretical analysis waveforms shown in Figure 7, it is clear that the critically stable waveforms of the simulation shown in Figure 9 are very similar to the waveforms in Figure 7. The changing tendencies of the ΔP , I_{td} and U_{dc} in the simulation are almost the same with the theoretical analysis, which means the analysis about the transient process of GCC in Section 3 is right. Since the theoretical waveforms are drawn qualitatively according to the mathematical model of GCC, the correctness of the mathematical model of GCC can also be verified. Meanwhile, when the system is critically stable, some key data of the simulation results and the corresponding theoretical analysis results are listed in Table 2. From the comparison of the simulation results and the theoretical analysis results, the imbalance power equation can be proved to be right. It can be seen that if the k_{vp} becomes larger, the errors become larger, too. Thus, the analysis of the effects of the damping term with k_{vp} can also be proved to be right. The deviation mainly comes from the neglect of the effects of the damping term related to k_{vp} . Moreover, the neglect of the controller's dynamics will have some influence on the results.

Table 2. Comparison of the Simulation Results and the Theoretical Results.

Quantity	MIPL (pu)/Simulation Results	MIPL (pu)/Imbalance Power Equation Results	
$k_{vp} = 6$	SCR = 1.9	0.754	0.734
$k_{vp} = 6$	SCR = 2.0	0.794	0.773
$k_{vp} = 7$	SCR = 2.0	0.795	0.773
$k_{vp} = 9$	SCR = 2.0	0.796	0.773

5.2. The Verification of the Effects of the Current Limitation

When the same voltage sag fault happens in the system with a current limiter, Figure 10 shows the waveforms of ΔP , I_{td} and U_{dc} under different conditions. In this case, the SCR and k_{vp} of this system is 2.0 and 6. The input power is 0.795 pu. The critical current limitation is 1.39. According to the simulation in the previous part, the system will become unstable without a current limiter.

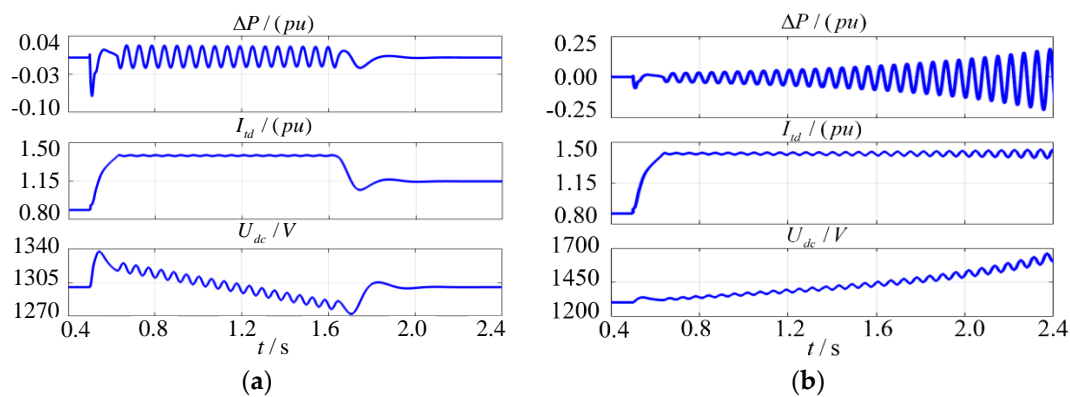


Figure 10. The effects of the current limitation: (a) the system is stable (current limitation is 1.38 pu); (b) the system is unstable (current limitation is 1.40 pu).

However, when the current limitation is smaller than the critical current limitation, such as 1.38. As shown in Figure 10a, the system finally becomes stable. Since the dynamics of the current loop exist in the real simulation, the waveforms of the ΔP , U_{dc} , and I_{id} are not constant during the period of the current limitation and they will fluctuate. If the current limitation is a little larger, such as 1.40. The DC voltage will become larger and larger. Finally, the system becomes unstable as shown in Figure 10b. Therefore, from the simulation results, the theoretical analysis about the effects of the current limitation can be proved right.

5.3. Experimental Results

Except for the simulation, hardware-in-the-loop (HIL) experiments based on the SpaceR are also applied. The SpaceR is a real-time simulation platform offering the complex-model-based design for an interaction with real-world environments. In the experiments, the system is simulated and the simulation of the system is separated into two parts: one is the simulated AC grid, another is the simulated GCC and equivalent line impedance. The SpaceR transfers the output of the simulated AC grid signals into real analog signals. One port of the SpaceR is used to output the analog signals of the AC grid. Taking another port of the SpaceR to act as the GCC and equivalent line impedance. Using a data line to connect the two ports and the experimental platform is built. Experimental platform is shown in Figure 11. The system model and its parameters are the same with the simulations.

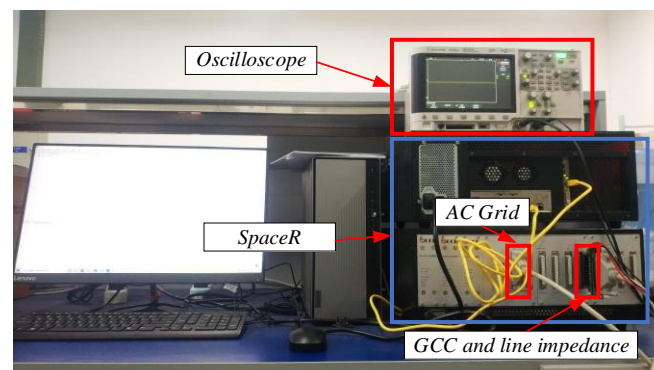


Figure 11. Experimental platform.

To verify the imbalance power equation, four cases are given here (the same with the simulations). The grid voltage drops from 1.0 pu to 0.9 pu when the remote voltage sag happens at $t = 0.5$ s. In these cases, the SCR and k_{vp} are 1.9 and 6, 2.0 and 6, 2.0 and 7, 2.0 and 9, respectively. The responses of the PCC phase A current (pu) are shown in Figure 12.

The experiment results are listed in Table 3. Comparing with the simulation results, it is clear that the experiment results are consistent with the simulations.

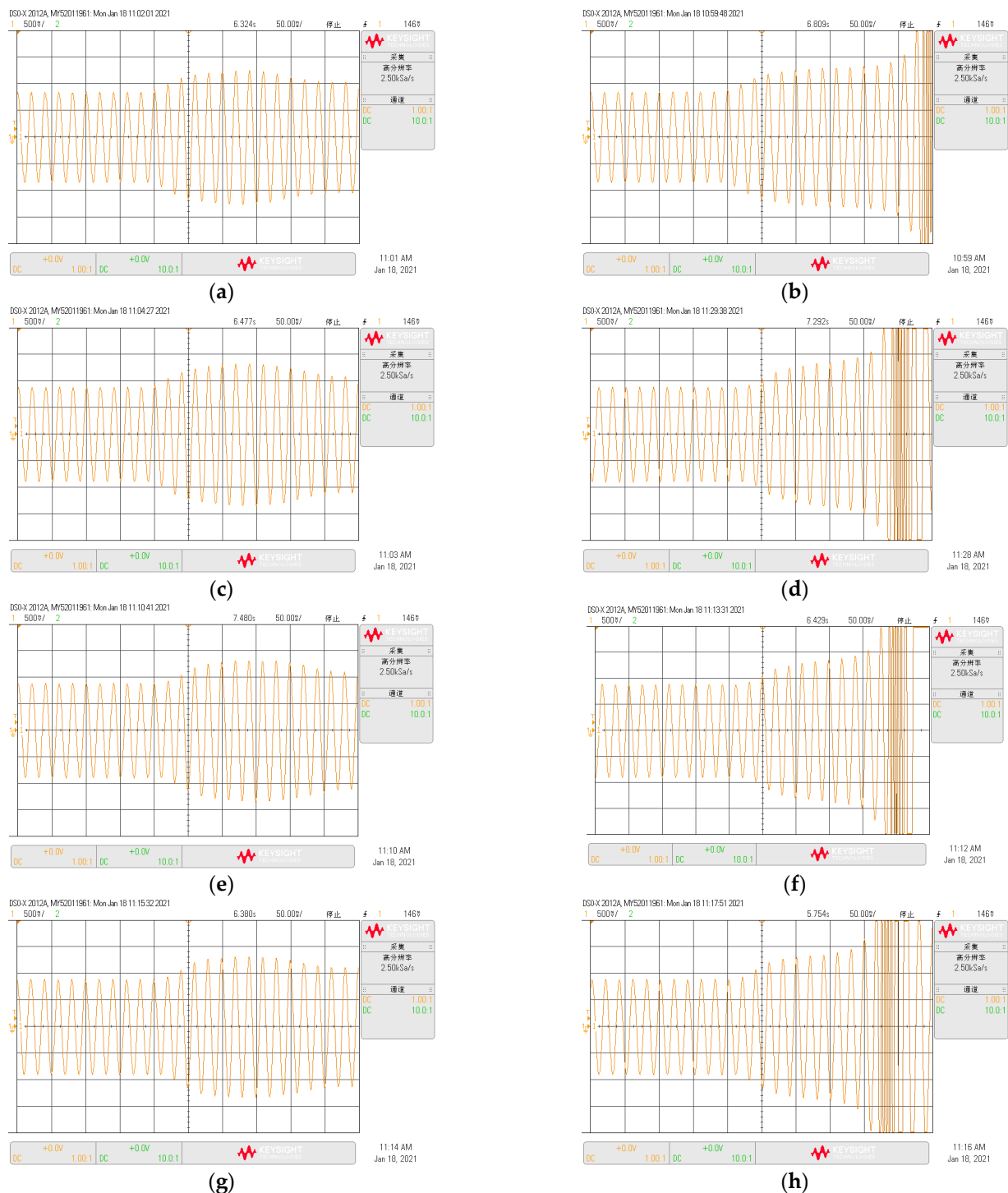


Figure 12. The responses of point of common coupling (PCC) phase A current (pu) when the remote voltage sag occurs: (a) The system is critically stable ($P_{in} = 0.752$ pu, $SCR = 1.9$, $k_{vp} = 6$); (b) The system is unstable ($P_{in} = 0.753$ pu, $SCR = 1.9$, $k_{vp} = 6$); (c) The system is critically stable ($P_{in} = 0.792$ pu, $SCR = 2.0$, $k_{vp} = 6$); (d) The system is unstable ($P_{in} = 0.793$ pu, $SCR = 2.0$, $k_{vp} = 6$); (e) The system is critically stable ($P_{in} = 0.793$ pu, $SCR = 2.0$, $k_{vp} = 7$); (f) The system is unstable ($P_{in} = 0.794$ pu, $SCR = 2.0$, $k_{vp} = 7$); (g) The system is critically stable ($P_{in} = 0.794$ pu, $SCR = 2.0$, $k_{vp} = 9$); (h) The system is unstable ($P_{in} = 0.795$ pu, $SCR = 2.0$, $k_{vp} = 9$).

Table 3. Experimental Results, Simulation Results and the Theoretical Results.

Quantity		MIPL (pu)/Experimental Results	MIPL (pu)/Simulation Results	MIPL (Pu)/Imbalance Power Equation Results
$k_{vp} = 6$	SCR = 1.9	0.752	0.754	0.734
$k_{vp} = 6$	SCR = 2.0	0.792	0.794	0.773
$k_{vp} = 7$	SCR = 2.0	0.793	0.795	0.773
$k_{vp} = 9$	SCR = 2.0	0.794	0.796	0.773

Moreover, to verify the effects of the current limitation, one case is given here (the same with the simulations). The SCR and k_{vp} of this system is 2.0 and 6. The input power is 0.795 pu. The responses of the DC voltage (pu) are shown in Figure 13. When the current limitation is 1.37, the system is stable. However, when the current limitation is 1.39, the system becomes unstable. That is also consistent with the simulations.

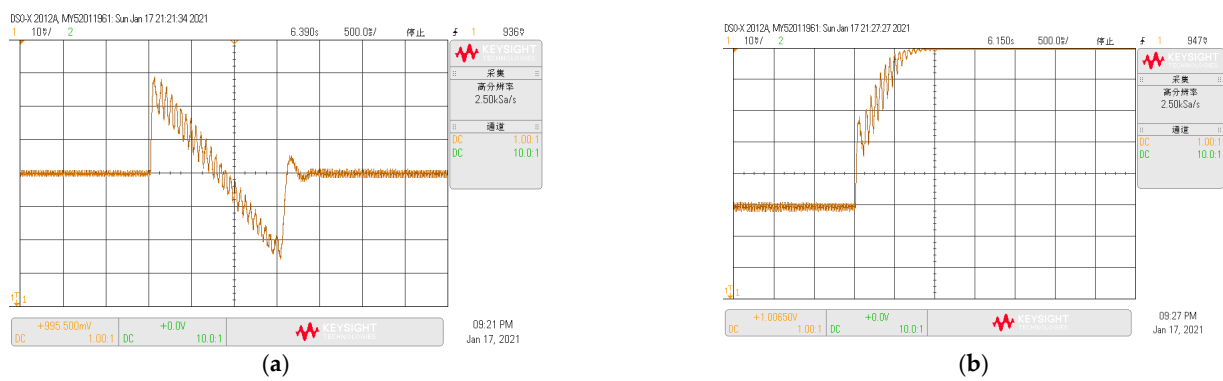


Figure 13. Responses of the DC voltage (pu) with the current limitation: (a) the system is stable (current limitation is 1.37 pu); (b) the system is unstable (current limitation is 1.39 pu).

6. Conclusions

In this paper, the mathematical models of the GCC and AC grid are first developed. Then, under the condition of the non-severe remote voltage sag, the influence of the imbalance power on the transient process of GCC is analyzed. To deal with the transient stability issues of the GCC caused by the imbalance power, the imbalance power equation of GCC is proposed in this paper. Meanwhile, the effects of the current limitation are also analyzed. The following conclusions can be drawn from this paper:

- (1) Based on the analysis of the equivalent AC circuit of GCC connected to the AC grid and the output power characteristics, the modeling of the AC grid is carried out. The mathematical model of the GCC that can be used to deal with the transient stability issues of GCC caused by the imbalance power is also developed. Furthermore, the transient process of GCC driven by the imbalance power is analyzed.
- (2) Different from some previous studies, this paper does not pay too much attention to the influence of PLL and the current loop during the transient process of the GCC. The transient stability issues will still exist even when the dynamics of these control loops are ignored, which means the key factor that will influence the transient stability of GCC is the imbalance power but not the influence of some control loops.
- (3) To keep the system operating stably after the non-severe remote voltage sag, there should be a maximum input power limit (MIPL) for the GCC. Meanwhile, the current limitation will also have some influence on the transient stability of the GCC. Based on the mathematical models of the GCC and the AC grid, the imbalance power equation of GCC is proposed in this paper and it can be used to determine the transient stability of the GCC.

In addition, the mathematical models of GCC and AC grid proposed in this paper are not only suitable for analyzing the transient stability of GCC under the condition of non-severe remote voltage sag, but they can also be applied to analyze the transient stability of GCC under other conditions, such as short circuit fault.

Author Contributions: Conceptualization, X.Q. and X.L.; methodology, X.Q. and X.L.; software, X.Q. and Y.Z.; validation, X.Q., Y.K., and X.L.; formal analysis, Y.K. and X.L.; investigation, X.Q. and X.L.; resources, X.Q. and Y.Z.; data curation, X.Q., and Y.Z.; writing—original draft preparation, X.Q., Y.K., and X.L.; writing—review and editing, X.Q., and X.L. All authors have read and agreed to the published version of the manuscript.

Funding: This research received no external funding.

Institutional Review Board Statement: Not applicable.

Informed Consent Statement: Not applicable.

Data Availability Statement: Not applicable.

Acknowledgments: This work is supported in part by the National Key Research and Development Program of China (2017YFB0902000), and in part by Science and Technology Project of State Grid (SGXJ0000KXJS1700841).

Conflicts of Interest: The authors declare no conflict of interest.

Abbreviations

P_{in}	The input power of the DC side.
P_{out}	The output power of the AC side.
U_{dc}	DC voltage of the DC side capacitor.
U_{dcref}	Reference of the DC side capacitor voltage.
I_t	Grid side AC current vector
I_{td}, I_{tq}	The d -axis and q -axis components of AC current under dq rotating reference frame.
I_{tdref}, I_{tqref}	The d -axis and q -axis reference value of AC current under dq rotating reference frame.
U_t	Point of common coupling (PCC) voltage vector.
U_g	Grid voltage vector.
θ_{pll}	Phase-locked loop (PLL) output angle in the stationary frame.
C	The DC side capacitor.
L_f, C_f	LC filter inductor and capacitor.
L_g	Grid-side line inductor.
X_g	Grid-side equivalent line impedance under the fundamental frequency.

References

- Blaabjerg, F.; Ma, K. Future on Power Electronics for Wind Turbine Systems. *IEEE J. Emerg. Sel. Top. Power Electron.* **2013**, *1*, 139–152. [[CrossRef](#)]
- Blaabjerg, F.; Zhe, C.; Kjaer, S. Power electronics as efficient interface in dispersed power generation systems. *IEEE Trans. Power Electron.* **2004**, *19*, 1184–1194. [[CrossRef](#)]
- Zhao, M.; Yuan, X.; Hu, J.; Yan, Y. Voltage Dynamics of Current Control Time-Scale in a VSC-Connected Weak Grid. *IEEE Trans. Power Syst.* **2016**, *31*, 2925–2937. [[CrossRef](#)]
- Wang, X.; Blaabjerg, F.; Wu, W. Modeling and Analysis of Harmonic Stability in an AC Power-Electronics-Based Power System. *IEEE Trans. Power Electron.* **2014**, *29*, 6421–6432. [[CrossRef](#)]
- Yang, D.; Ruan, X.; Wu, H. Impedance Shaping of the Grid-Connected Inverter with LCL Filter to Improve Its Adaptability to the Weak Grid Condition. *IEEE Trans. Power Electron.* **2014**, *29*, 5795–5805. [[CrossRef](#)]
- Zhang, L.; Harnefors, L.; Nee, H. Interconnection of two very weak ac systems by VSC-HVDC links using power-synchronization control. *IEEE Trans. Power Syst.* **2011**, *26*, 344–355. [[CrossRef](#)]
- Wu, H.; Wang, X. Design-Oriented Transient Stability Analysis of Grid-Connected Converters with Power Synchronization Control. *IEEE Trans. Ind. Electron.* **2019**, *66*, 6473–6482. [[CrossRef](#)]
- Wu, H.; Wang, X. Design-Oriented Transient Stability Analysis of PLL-Synchronized Voltage-Source Converters. *IEEE Trans. Power Electron.* **2020**, *35*, 3573–3589. [[CrossRef](#)]
- Hu, Q.; Fu, L.; Ma, F.; Ji, F. Large Signal Synchronizing Instability of PLL-Based VSC Connected to Weak AC Grid. *IEEE Trans. Power Syst.* **2019**, *34*, 3220–3229. [[CrossRef](#)]

10. Dong, D.; Wen, B.; Boroyevich, D.; Mattavelli, P.; Xue, Y. Analysis of phase locked loop low frequency stability in three phase grid connected power converters considering impedance interactions. *IEEE Trans. Ind. Electron.* **2015**, *62*, 310–321. [[CrossRef](#)]
11. Zhang, C.; Cai, X.; Li, Z.; Rygg, A.; Molinas, M. Properties and physical interpretation of the dynamic interactions between voltage source converters and grid: Electrical oscillation and its stability control. *IET Power Electron.* **2017**, *10*, 894–902. [[CrossRef](#)]
12. Ledesma, P.; Usaola, J. Doubly Fed Induction Generator Model for Transient Stability Analysis. *IEEE Trans. Energy Convers.* **2005**, *20*, 388–397. [[CrossRef](#)]
13. Huang, L.; Xin, H.; Wang, Z.; Zhang, L.; Wu, K.; Hu, J. Transient Stability Analysis and Control Design of Droop-Controlled Voltage Source Converters Considering Current Limitation. *IEEE Trans. Smart Grid* **2019**, *10*, 578–591. [[CrossRef](#)]
14. Xin, H.; Huang, L.; Zhang, L.; Wang, Z.; Hu, J. Synchronous Instability Mechanism of P-f Droop-Controlled Voltage Source Converter Caused by Current Saturation. *IEEE Trans. Power Syst.* **2016**, *31*, 5206–5207. [[CrossRef](#)]
15. Huang, L.; Zhang, L.; Xin, H.; Wang, Z.; Gan, D. Current limiting leads to virtual power angle synchronous instability of droop-controlled converters. In Proceedings of the IEEE-Power-and-Energy-Society General Meeting (PESGM), Boston, MA, USA, 17–21 July 2016.
16. Kaban, M.; Singh, P.; Niebur, D. Large Signal Lyapunov-Based Stability Studies in Microgrids: A Review. *IEEE Trans. Smart Grid* **2017**, *8*, 2287–2295. [[CrossRef](#)]
17. Goksu, O.; Teodorescu, R.; Bak, C.L.; Iov, F.; Kjaer, P.C. Instability of Wind Turbine Converters During Current Injection to Low Voltage Grid Faults and PLL Frequency Based Stability Solution. *IEEE Trans. Power Syst.* **2014**, *29*, 1683–1691. [[CrossRef](#)]
18. Yang, Z.; Ma, R.; Cheng, S.; Zhan, M. Nonlinear Modeling and Analysis of Grid-Connected Voltage-Source Converters Under Voltage Dips. *IEEE J. Emerg. Sel. Top. Power Electron.* **2020**, *8*, 3281–3292. [[CrossRef](#)]
19. Huang, M.; Wong, S.-C.; Tse, C.K.; Ruan, X. Catastrophic Bifurcation in Three-Phase Voltage-Source Converters. *IEEE Trans. Circuits Syst. I Regul. Pap.* **2013**, *60*, 1062–1071. [[CrossRef](#)]
20. Huang, M.; Peng, Y.; Tse, C.K.; Liu, Y.; Sun, J.; Zha, X. Bifurcation and Large-Signal Stability Analysis of Three-Phase Voltage Source Converter Under Grid Voltage Dips. *IEEE Trans. Power Electron.* **2017**, *32*, 8868–8879. [[CrossRef](#)]
21. Strogatz, S. Phase Plane. In *Nonlinear Dynamics and Chaos*, 2nd ed.; Westview: Boulder, CO, USA, 2015; pp. 301–331.
22. Heffron, G.; Phillips, A. Effect of a modern amplidyne voltage regulator on underexcited operation of large turbine generators. *Power App. Syst. Part III Trans. Amer. Inst. Elect. Eng.* **1952**, *71*, 692–697. [[CrossRef](#)]
23. Moussa, M.; Yu, N. Dynamic interaction of multi-machine power system and excitation control. *IEEE Trans. Power App. Syst.* **1974**, *93*, 1150–1158. [[CrossRef](#)]
24. Xiong, L.; Zhuo, F.; Wang, F.; Liu, X.; Chen, Y.; Zhu, M.; Yi, H. Static Synchronous Generator Model: A New Perspective to Investigate Dynamic Characteristics and Stability Issues of Grid-Tied PWM Inverter. *IEEE Trans. Power Electron.* **2016**, *31*, 6264–6280. [[CrossRef](#)]
25. Zhong, C. Synchronverters: Inverters that mimic synchronous generators. *IEEE Trans. Ind. Electron.* **2011**, *58*, 1259–1267. [[CrossRef](#)]
26. Shintai, T.; Miura, Y.; Ise, T. Oscillation Damping of a Distributed Generator Using a Virtual Synchronous Generator. *IEEE Trans. Power Deliv.* **2014**, *29*, 668–676. [[CrossRef](#)]
27. Yuan, H.; Yuan, X.; Hu, J. Modeling of Grid-Connected VSCs for Power System Small-Signal Stability Analysis in DC-Link Voltage Control Timescale. *IEEE Trans. Power Syst.* **2017**, *32*, 3981–3991. [[CrossRef](#)]